SIMULATING THE ROTATIONAL DYNAMICS OF TIANGONG-1 FOR RE-ENTRY ANALYSIS

L. Sagnières[1], M. K. Jørgensen[2], and I. Sharf[3]

[1]*Department of Mechanical Engineering, McGill University, Montréal, Québec, Canada and IMCCE, Observatoire de Paris, PSL Research University, CNRS, Sorbonne Université, Université de Lille, Paris, France, luc.sagnieres@mail.mcgill.ca*

[2]*Department of Mechanical Engineering, McGill University, Montréal, Québec, Canada, Mikkel.Jorgensen@mail.mcgill.ca*

[3]*Department of Mechanical Engineering, McGill University, Montréal, Québec, Canada, Inna.Sharf@mcgill.ca*

ABSTRACT

Tiangong-1, launched in September 2011, re-entered Earth's atmosphere on April 2, 2018. As part of the research presented in this paper, Tiangong-1 is used as a case study to analyse the rotational dynamics of large debris during final descent and its influence on re-entry predictions such as time and location of impact. Satellite laser ranging observations and radar images have shown that in the months preceding its re-entry, the rotation of Tiangong-1 accelerated. Using the Debris Spin/Orbit Simulation Environment (D-SPOSE), simulations are conducted of the satellite's rotational motion to provide a better understanding of its attitude dynamics during the last weeks of its life and to narrow down the values of the relevant, but uncertain parameters. It is shown that the aerodynamic torque is responsible for the witnessed angular acceleration due to a complex interaction with the gravity-gradient torque. With the results of the rotational motion analysis in hand, we proceed to study the effect of the spacecraft rotational motion on its altitude in the last few days of its descent to Earth. In particular, the short-term effects of the changing cross-sectional area of Tiangong-1, found to be decreasing with time as a result of its rotational motion, on the predicted time and location of re-entry are presented.

Keywords: Tiangong-1; space debris; attitude dynamics; descent; re-entry; propagation.

1. INTRODUCTION

There are a high number of large pieces of space debris in lower Earth orbit, and some are bound to re-enter Earth's atmosphere sooner rather than later. Due to their size, mass, and material composition, some of these pieces of debris will survive re-entry and impact Earth, posing a potential threat to life and infrastructure on the ground. A lot of effort is therefore dedicated to tracking high-risk debris and predicting their orbital evolution and re-entry path. One example of such debris was the first Chinese space station, Tiangong-1, which was launched in September 2011. After almost five years of service, it was decommissioned in March 2016. As orbit maintenance manoeuvres stopped, its altitude slowly decayed, from an initial altitude of approximately 380 km, until it re-entered Earth's atmosphere over the Pacific Ocean on April 2, 2018 at 00:15 UTC.

Tiangong-1 was the focus of many observation campaigns during its final months, mostly in order to accurately predict its time and place of re-entry. Early re-entry predictions were made in 2017 by Choi et al. [1] based on observed TLE data, using various tools for re-entry analysis including debris assessment software (DAS) and the debris risk assessment and mitigation analysis (DRAMA) software. The simulation was initiated on the 11th of September 2017 and predicted the re-entry of Tiangong-1 on approximately the 3rd of February 2018 with an impact location in the middle of the Atlantic ocean. For these simulations the drag coefficient of Taingong-1 was assumed to be 2.2 and the cross-sectional area was set to 17 m^2. On-going observation campaigns were carried out through the Italian component of the European Space Surveillance and Tracking (SST) [7] [13]. Re-entry predictions made in the first two months of 2017 as a result of this campaign suggested the first week of April 2018 as the re-entry window. Refined predictions made after a G2 solar storm in March 2018 then gave a re-entry window spanning 01/04/2018 01:00 - 02/04/2018 01:00. The final re-entry prediction was made 9 hours prior to impact and the approximated impact epoch was 02/04/2018 00:44 ± 2.62 h. During this observational campaign, it was also possible to estimate the average cross-sectional area of the station. The estimated values for the area used to calculate the ballistic coefficient were 65 m^2 on the 9th of February 2017, 40 m^2 on the 11th of February 2018, and 26 m^2 on the 1st of April 2018. The large differences in observed areas contributed to the uncertainty of the re-entry predictions. In addition, a campaign combining observations for the purpose of studying re-

entry has been carried out by the European Space Agency (ESA) [14], in which Tiangong-1 is used as a case study. As part of this campaign, TIRA radar observations, European and Chinese SLR observations, Santorcaz radar observations and MMT optical sensor observations were combined and re-entry predictions were made based on this data and compared to re-entry predictions made in "real time". The real time predictions were carried out as Tiangong-1 was descending/re-entering, whereas the predictions based on observations were carried out a-posteriori with multiple data sources. Combined TIRA and SLR predictions were compared to real time predictions with orbital data available up until 31/03/2018 06:54. The combined observational data predicted impact at 02/04/2018 00:05 whereas the real time prediction gave 01/04/2018 23:25. Furthermore, all observations combined were compared to real time predictions, with orbital data available up until 01/04/2018 06:19. The combined observational data and the real time prediction estimated the impact times at 02/04/2018 00:46 and 02/04/2018 01:27, respectively. Another observation made in [14] suggests the main source of uncertainty during the campaign was the predicted solar activity, which, compared to the observed solar activity, altered the re-entry prediction by almost 24 hours, 3 days prior to re-entry.

A-posteriori predictions were also put forward from TLE time series analysis using the Semi-analytic Tool for End of Life Analysis (STELA) software [2]. This study provides re-entry predictions using the observations available at several dates from December 2017 up to a few days before impact and shows dates of re-entry that consistently occur too early compared to the actual time and date of impact. It also presents ballistic coefficients calculated from fitting the TLE data over the 30 days before the dates when the predictions are made. Similarly to the SST results in [7], the study shows that the station's corresponding cross-sectional area decreases with time.

In addition to observations of the station's orbital motion, some observations were also made of the satellite's rotational motion. This is particularly opportune as there is a dearth of studies related to the rotational dynamics of space objects at such low altitudes, and the long-term effect of the atmosphere on a satellite's angular motion has rarely been analyzed in detail. Moreover, the impact that a satellite's rotation has on its descent and re-entry trajectories is unknown; most orbital decay studies disregard the rotational motion of the object completely and assume a constant cross-sectional area. The observations of Tiangong-1's rotation therefore provide a valuable pool of information for modellers who study the attitude dynamics of large inoperative spacecraft and for those who track them for re-entry predictions.

Two observation campaigns specifically studied Tiangong-1's attitude motion during the last few months before re-entry. First, the Tracking and Imaging Radar (TIRA) telescope tracked the station, providing estimates of its angular velocity direction and magnitude [12]. Second, as Tiangong-1 contained multiple corner curve reflectors (CCR), satellite laser ranging (SLR) was similarly used to obtain values of its spin period and spin axis direction [6]. That study concluded that the observed spin-up of the satellite was due to an atmospheric density gradient torque. Fig. 1 shows the two observational data sets over the last year of its life; these will serve to constrain the determination of certain parameters of Tiangong-1 later in this paper.

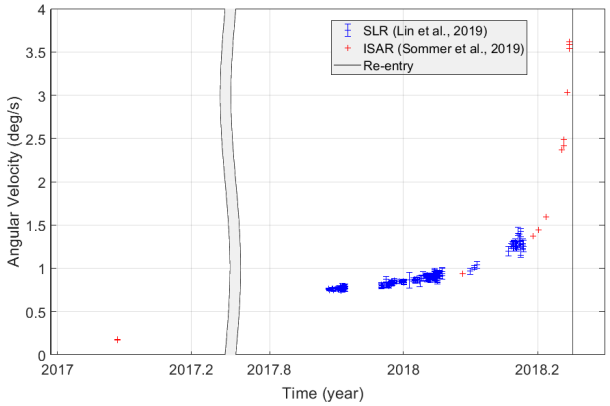

Figure 1: Angular velocity observations of Tiangong-1

Using two different modeling tools, this paper will attempt to develop a better understanding of the descent dynamics and re-entry of large space debris, focusing on the effects of rotational motion, by using Tiangong-1 as a case study. First, the Debris SPin/Orbit Simulation Environment (D-SPOSE) will be used to investigate the rotational motion of Tiangong-1 during its descent from the altitude of approximately 300 km to an altitude of $\sim$120 km (at perigee). The latter corresponds to what is typically considered as the onset of re-entry: from this point, Tiangong-1 took 3.8 hours to reach the Earth's surface, as estimated with the Debris Risk Assessment and Mitigation Analysis (DRAMA) software. D-SPOSE is an open-source software containing a high-fidelity coupled orbit-attitude propagator dedicated to the study of the long-term evolution of the attitude motion of large space debris [11, 10]. Second, re-entry predictions will be presented by employing DRAMA—a software suite developed by ESA for space debris mitigation [4].

In Section 2, the various parameters of the station used as model inputs into D-SPOSE are described. In Section 3, the investigation into Tiangong-1's rotational motion over the period of approximately four months before re-entry is presented. In Section 4, the influence of the satellite's rotational motion on re-entry predictions is analyzed. This involves propagating the motion of Tiangong-1 with D-SPOSE over the last few days of its life and using relevant information in DRAMA analyses to determine its impact time and locations. Finally, Section 5 will present the major conclusions from this study.

2. MODEL INPUTS

In order to correctly assess the rotational dynamics of Tiangong-1 during re-entry, a valid model of the spacecraft needs to be adopted. Fig. 2 shows the tessellated surface geometry used as input into D-SPOSE. It contains 168 surfaces and follows the dimensions as displayed by Lin et al. [6]: a body measuring 10.4 m in length and with a diameter of 3.35 m; and solar panels measuring 7 m by 3 m, and in an orientation parallel to the x-y plane, similarly to what was found from ISAR images [12]. The origin of the reference frame in Fig. 2 is the assumed center of mass, located +4 m from the center of the circular surface at the end of the -x-axis. The principal body-frame axes are shown in red. The spacecraft is assumed to have a mass of 8500 kg. A diagonal inertia matrix with $I_x = 16403.01\ kg \cdot m^2$, $I_y = 70915.56\ kg \cdot m^2$, and $I_z = 76392.38\ kg \cdot m^2$ is adopted [6]. Uncertainty on the moments of inertia and the location of the center of mass will be assessed in Section 3.

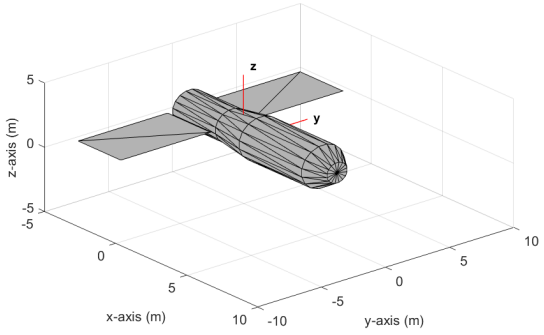

Figure 2: Tessellated model of Tiangong-1 in the body-fixed frame used for propagation in D-SPOSE

The largest external perturbations affecting the attitude dynamics of satellites at the altitudes of Tiangong-1 are the aerodynamic torque, the gravity-gradient torque, and internal energy dissipation. Simulations were run using D-SPOSE including these three torques, as well as aerodynamic drag and third-body perturbations for orbital motion. EGM2008 was used as the geopotential model up to degree and order 6 for the calculation of the Earth's gravitational field and the gravity-gradient torque [8]. NRLMSISE-00 was used to obtain the atmospheric density at the satellite position throughout the propagations, using the observed values of the solar and geomagnetic activity proxies, A_p and $F_{10.7}$, and similarly HWM14 was used to obtain high altitude winds [9, 3]. Preliminary simulations using D-SPOSE showed that the classical value of $c_D = 2.2$ overestimated the aerodynamic drag leading to a much quicker orbital decay than the observations (by approximately 2-3 weeks). Therefore, a value of 1.9 was chosen for the following simulations. Internal energy dissipation was modelled with a Kane damper taking a damping coefficient of $k_d = 1\ kg \cdot m^2 \cdot s^{-1}$ and a diagonal inertia tensor with $I_d = 1\ kg \cdot m^2$.

A TLE from the time of the first SLR observation of the station, on November 21, 2017, when Tiangong was orbiting at approximately 300 km, was used to initialize propagations with D-SPOSE:

$$1\ \ 37820U\ \ 11053A\ \ 17325.44940311\ \ .00055570\ \ 94008-5\ \ 16563-3\ \ 0\ \ 9996$$
$$2\ \ 37820\ \ \ 42.7550\ \ 309.2976\ \ 0017835\ \ 127.1604\ \ 9.2509\ \ \ 15.92062358352912$$

The simulations lasted until atmospheric re-entry was achieved (at an altitude of 120 km) propagating with a time step of $0.05\ s$. Such a short time step was used to capture the full effect of the aerodynamic torque over one spacecraft rotation. At the time of the TLE, according to SLR observations, the spacecraft is in a prograde spin with an angular velocity of 0.75 $\deg \cdot s^{-1}$ about its body-frame z-axis, that is its major principal axis, and nutating approximately 23 $\deg$ away from the orbit normal [6]. These values were therefore used to initialize the attitude and angular velocity of Tiangong-1 at the time of the TLE. The actual position of the spin axis about the 23 $\deg$ cone centered at the orbit normal and the exact orientation of the spacecraft about its spin axis did not have a noticeable effect on the long-term propagations.

3. ROTATIONAL DYNAMICS OF TIANGONG-1

As little information is publicly available about Tiangong-1, the analysis of its rotational motion using D-SPOSE requires an in-depth investigation into parameters affecting its attitude evolution. Specifically, in Section 3.1, we discuss the uncertainties present in the geometry and inertia properties of the spacecraft and present investigatory simulation results to bound these uncertainties. In Section 3.2, we then summarize the findings on the key aspects of the satellite's complex rotational motion. Finally, an analysis of the evolution of the spacecraft's cross-sectional area is presented in Section 3.3.

3.1. Parameter Uncertainty Analysis

One of the largest uncertainties in the calculation of the aerodynamic torque on the station is the surface geometry model of the spacecraft, i.e., the size and shape of the body, as well as the position of the center of mass in that body. Although the size and shape of the spacecraft are relatively well known, the exact location of the center of mass is not. Simulations were therefore performed varying the location of the center of mass from the position shown in Fig. 2, keeping the values of the moments of inertia constant. The largest differences occurred by varying the center of mass along the body-frame y-axis, and this is illustrated in Fig. 3 for the angular velocity response of the station.

From these results, it can be seen that the evolution of the satellite's angular velocity is very sensitive to the location of the center of mass. Depending on where it is in the surface geometry model, the effect of the aerodynamic torque will either lead to an initial increase or decrease

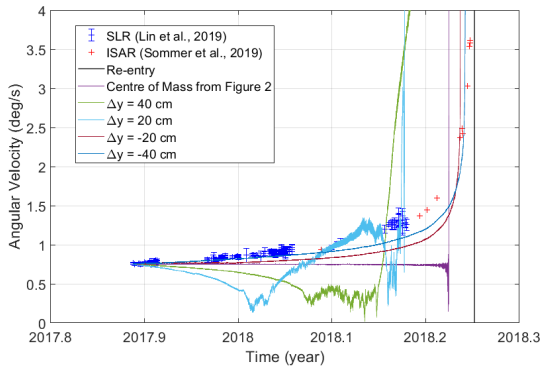

Figure 3: Evolution of angular velocity magnitude when varying the center of mass

of the angular velocity for the first couple of months of the propagation. When the center of mass is on the +y side of the center of the cylindrical body, $\Delta y = 20$ cm and $\Delta y = 40$ cm in Fig. 3, the angular velocity response is drastically different from observations: the spacecraft rotation rate first decays over a few weeks and then, the station starts tumbling and enters a different attitude state where an increase occurs. When the center of mass is along the symmetry axis of the spacecraft (see Fig. 3, response Center of Mass from Fig. 2), the net effect of the aerodynamic torque is zero, until the very end of the propagation when atmospheric densities, and in turn the related aerodynamic torque, are much higher, leading to a chaotic motion. For the center of mass on the -y side of the center of the cylindrical body, an evolution of the satellite's angular velocity matching closely what is seen by observations occurs, indicating that this is the most likely scenario. Multiple simulations were also performed shifting the center of mass along the x-axis and z-axis. Moving the center of mass along the z-axis by ± 50 cm showed negligible differences, while shifting it along the +x-axis by 1 and 2 m did not change the overall tendency of the angular velocity increase, but did modify the shape of the evolution slightly.

Comparison of semi-major axis and angular velocity responses from these simulations indicates that the very fast spin-up of the spacecraft at the end of the propagation coincides with its re-entry time in every scenario. This spin-up occurs at different times for each simulation due to the different angular motions leading to different cross-sectional areas, in turn leading to different times of orbital decay due to the varying effect of aerodynamic drag. This will also be the case for the following simulations. However, for gaining a better understanding of Tiangong-1's rotational dynamics, it is the general shape of evolution of the satellite's angular velocity that is important, and not finding the parameters that will lead to a perfect agreement with observations.

The second largest parameter uncertainty that has the potential to significantly alter the evolution of the satellite's attitude dynamics is in the moments of inertia of the satellite. Different values of the moments of inertia will change the way the gravity-gradient torque affects the motion of the satellite's spin axis, in turn leading to a different evolution of the angular velocity. Simulations were performed by varying I_z by $\pm 5\%$, for the scenario where the center of mass of the spacecraft is located 20 cm along the -y-axis from the position in Fig. 2. From these simulations, shown in Fig. 4, we can see that the shape of the angular velocity increase is indeed altered.

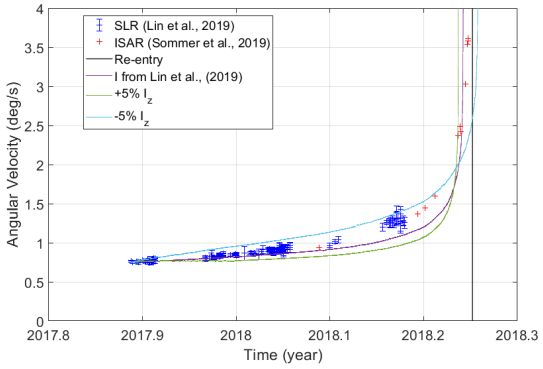

Figure 4: Evolution of angular velocity magnitude when varying major moment of inertia

3.2. Spin Axis Motion

The differences in the evolution of the satellite's angular velocity seen in Figs. 3 and 4 are due to the complex interaction between the aerodynamic and gravity-gradient torques and the various periods present in the dynamics of the spacecraft. Its rotational motion is influenced by several underlying phenomena, each characterized by a period and affecting the satellite in different ways, in particular:

1. The **period of rotation** of the satellite about its center of mass is on the order of **480 seconds** ($0.13\bar{3}$ h) at the beginning of our propagations (November-December 2017). The effect of the aerodynamic torque can either be positive or negative at any instant, where an increase of the angular velocity occurs when one side of the satellite is in view of the atmospheric flow or a decrease when the other side is in view.

2. The gravity-gradient torque forces a closed-loop motion of the satellite's spin axis about the orbit normal, which in turn precesses with the orbit due to the Earth's oblateness ($\approx$ once per year). This **nutation motion** of the spin axis depends on the satellite's moments of inertia, orbit, and angular velocity, and for Tiangong-1 has a period of approximately **31 hours** at the beginning of the simulations. Because the spin axis orientation changes over this time frame, the orientation of the surfaces encountered by the atmospheric flow will vary and the resulting aerodynamic torque will also be different.

3. The **orbital period** of the satellite, approximately **90 minutes** (1.5 hours), also needs to be considered. Because the altitude of the spacecraft oscillates over one orbital period due to Earth's oblateness, the atmospheric density encountered will not be the same, and the effect of the aerodynamic torque will therefore oscillate over one orbit. Furthermore, the spin axis of Tiangong-1 is relatively fixed in the inertial frame over the time scale of one orbit (compared to the 31 hour nutation of the spin axis). A relative rotation of the spin axis with respect to the incoming air flow will therefore occur as the satellite orbits Earth, changing the orientation of the satellite surfaces encountered by the atmosphere, and hence the influence of the aerodynamic torque.

All of these motions influence the satellite's attitude dynamics in a complex way, leading to the various evolutions of the angular velocity as was observed in Figs. 3 and 4. If the satellite did not rotate about a relatively stable axis, then a tumbling would eventually occur; if the relative rotation of the airflow with respect to the spin axis did not occur due to both the nutation and orbital motion, and if the density was constant, then the symmetry of the spacecraft body would lead to an average aerodynamic torque of zero. It is the combination of these motions, and the fact that the center of mass of the spacecraft is not along its symmetry axis, that lead to a non-zero net effect. The exponential increase of the angular velocity seen throughout the simulations in the -y configuration is then simply due to the exponential increase in atmospheric density, as the satellite's altitude decreases, that leads to a larger effect of the aerodynamic torque.

In all, the results of Sections 3.1 and 3.2 demonstrate that the spin-up observed during the spacecraft re-entry is indeed due to the aerodynamic torque, and that the center of mass of the station is most likely positioned on the -y side (20-40 cm) of the cylindrical body, while the moment of inertia is likely a few percent below the value reported in Lin et al. [6]. Furthermore, unlike what has been concluded by Lin et al. [6], it is *not* necessary to account for an atmospheric density gradient torque: considering a constant atmospheric density over the satellite body at a given time is enough for the classical aerodynamic torque to explain the evolution of angular velocity observed from SLR and ISAR images.

3.3. Cross-Sectional Area Analysis

In order to obtain a complete understanding of the effect of Tiangong-1's rotational motion on the satellite's orbit during its descent, a closer look at the motion of the spin axis and the evolution of the spacecraft's cross-sectional area in the weeks before re-entry is needed. As shown in the previous sections, the motion of Tiangong-1's spin axis depends on its initial orientation and orbit, and on the station's major moment of inertia and location of the center of mass. Nevertheless, over the propagation time frame, simulations have shown that its motion evolves in a similar way for every simulation performed. Therefore, in the rest of the paper, in this Section as well as in Section 4, the parameter values which provided a closest fit between the simulated response and the observations are used for analysis, which will be referred to as the baseline scenario. As shown in Section 3.1, this corresponds to the simulation where the center of mass is at $\Delta y = -20$ cm from the position in Fig. 2, using the input information from Section 2, and using the exact moments of inertia from Lin et al. [6].

Figure 5 shows the evolution of the spin axis motion over the propagation time frame. Initially, the spin axis nutates about 23° away from the orbit normal with a period of 31 hours. As angular velocity increases, the angular difference between the satellite's angular velocity vector and the orbit normal slowly decreases, and its associated (nutation) period increases. The angular difference between the angular velocity vector and the orbit normal (the nutation angle) is represented in blue, while the period of the motion is shown in red. One can observe that the nutation angle oscillates. This is due to the fact that the motion of the angular velocity vector about the orbit normal is not circular, but contains a small libration on the order of 1.7 deg with the same period as the nutation. Put differently, the center of the circular motion of the spin axis is offset from the orbit normal by approximately 1.7 deg: this is expected due to the gravitational torque.

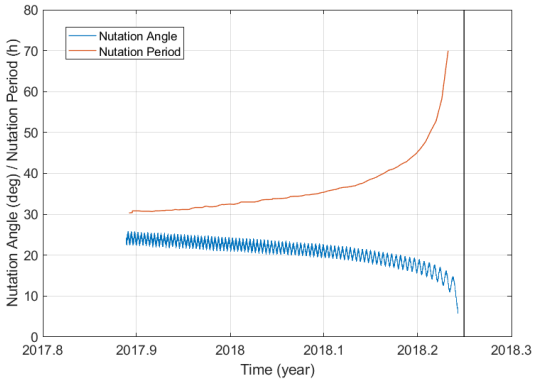

Figure 5: Evolution of the spin axis motion for the baseline scenario

As noted earlier, in light of the particular evolution of the spin axis, the cross-sectional area of the satellite with respect to the incoming airflow will vary with time. This is illustrated in Fig. 6, where the satellite's cross-sectional area A is presented. The three curves show the evolution of the satellite's cross-sectional area over a period of 6 hours for three different days throughout its propagation. One can see the high-frequency oscillations due to the satellite's rotation and the low-frequency ones due to the relative motion of the spin axis with respect to the incoming air flow over approximately one half-orbit. These motions evolve throughout the simulation, and while the cross-sectional area can vary between 10 and 50 m^2 at

the initial epoch on November 21, 2017, the maximum value of A decreases with time, decreasing to 40 m^2 by March 29, 2018. As the angular velocity increases, the frequency of the high-frequency oscillations due to the satellite's rotation also increases. However, the oscillations due to relative motion of the spin axis maintain their characteristic period, approximately equal to half of the orbital period. The decrease of the maximum cross-sectional area is due to the decrease of the nutation angle as the spin axis (the body-frame z-axis) moves closer to the orbit normal, leading to a smaller possible cross-sectional area of some of the surfaces, including the solar panels. One can see this more clearly in Fig. 7, which displays the evolution of the mean cross-sectional area of Tiangong-1, as a moving average over three days, and which shows a non-negligible decrease with time. This new information may partially explain the errors in estimates of the satellite's re-entry time when a constant cross-sectional area is assumed, as in [1] and [2], and is consistent with the decreasing estimates of the satellite's cross-sectional area found in previous studies [2, 7].

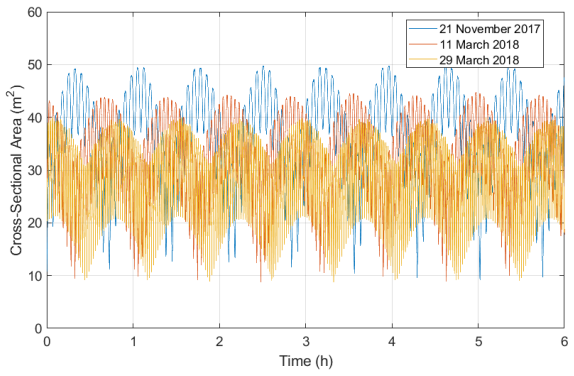

Figure 6: Tiangong-1's cross-sectional area for baseline scenario

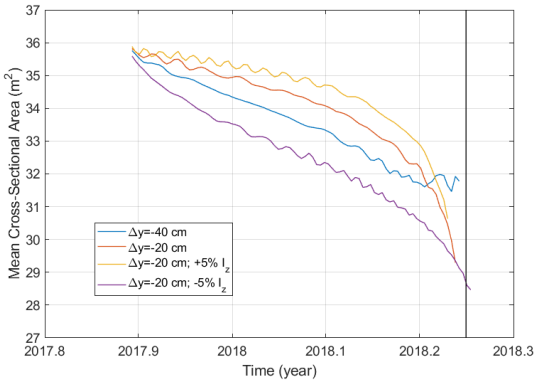

Figure 7: Tiangong-1's mean cross-sectional area averaged over three days

4. SHORT-TERM EFFECTS OF ROTATIONAL MOTION ON RE-ENTRY

Now that we have narrowed the uncertain parameter values of Tiangong-1, and shown that the station's evolving rotational motion leads not only to the expected time-varying cross-sectional area, but also to a noticeable decrease of the area moving average over time, we will use D-SPOSE to estimate the influence of the rotational motion on the satellite's orbital decay and on the predictions of its re-entry time and location. This will be done for a short propagation time frame, on the order of several days before the station's actual re-entry. In particular, in Section 4.1, four sets of simulations are presented to highlight the differences between coupled orbit-attitude propagation and orbital only propagation in terms of descent time and the resultant debris location at the onset of re-entry. Then, in Section 4.2, we employ DRAMA to investigate its predictions of Tiangong-1's impact location for several values of the specified cross-sectional area of the station in view of the oncoming aerodynamic flow. The schematics of D-SPOSE and DRAMA analyses are illustrated in Fig. 12 to clarify the information flow and connections between the two. Finally, in Section 4.3, the previously suggested notion that solar activity is a significant source of uncertainty on the re-entry predictions of Tiangong-1 is assessed. To do so, simulations are carried out to compare the descent of the station over three days before re-entry, by using fixed vs. measured solar indices.

4.1. Coupled attitude-orbit propagation vs. orbital only propagation

We proceed to study the short-term effects of the rotational motion of Tiangong-1, more specifically, its changing cross-sectional area, on the re-entry predictions. To this end, D-SPOSE is used to conduct simulations of the station's rotational and translational motion to provide a clear picture of the changes in its effective cross-sectional area during the last days of its life. Two sets of results are obtained with D-SPOSE: for coupled orbital-attitude propagation (hence, time-varying area) versus using D-SPOSE for orbital propagation only (with constant cross-sectional area). These simulations as carried out for the baseline parameters of the station, that is, with the center of mass at $\Delta y = -20$ cm from the position in Fig. 2. For the orbital only simulations, the effects of aerodynamic torque, gravity gradient torque, and internal energy dissipation are not considered.

Propagation results starting with one day, three days and seven days prior to the actual impact time (02/04/19 00:15:00) are presented. The aforementioned effects on re-entry are quantified in terms of the difference in time and location of the debris, at the point of re-entry, between modelling a time-varying cross-sectional area and assuming a constant time-averaged cross-sectional area over the same time period and with the same initial conditions. The initial conditions for the three aforementioned

propagations are provided in Table 1. An additional propagation starting one day before impact, denoted by "1*", is presented to highlight the effect of the initial debris attitude on the re-entry results. The initial orbital elements and the time of initiation of the propagation are defined by observational data from TLEs. All initial angular velocities and attitudes (with the exception of the 1* case) are defined by using the corresponding values from the long-term propagation results from Section 3, taken one, three, and seven days before the predicted impact for the one-, three-, and seven-day propagations, respectively.

As already noted, for each propagation (one, three, and seven days before impact), two types of simulations are conducted. First, coupled orbit-attitude propagation is conducted and the cross-sectional area responses of Tiangong-1 for each propagation are presented in Fig. 8. The mean values of the cross-sectional area time history for each of these propagations are used as the fixed area parameter for the corresponding orbital only propagations; these values are provided in Table 2 and we notice they differ by less than 1%.

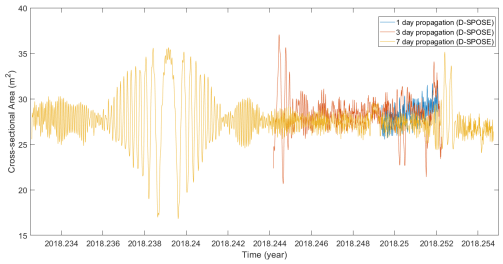

Figure 8: Tiangong-1's cross-sectional area during orbit-attitude propagation (1-hour moving average)

The effects of accounting for time-varying cross-sectional area and the initial orientation on the altitude evolution during Tiangong-1 re-entry are illustrated in Fig. 9 for all propagations. The exact re-entry times are provided in Table 2 and the locations of Tiangong-1 post propagation (at the boundary of re-entry) are illustrated in Fig. 10. For the one- and three-day propagations, the predicted re-entry times are quite close for the time-varying and fixed cross-sectional area simulations, differing by $0.3\bar{3}$ h (time-varying result leading) and $0.1\bar{6}$ h (time-varying result lagging), respectively. The difference in re-entry time for the one-day propagation is larger than that of the three day propagation. This is unexpected; however, the difference is only 20 vs. 10 minutes. For the seven-day propagation, this discrepancy is considerably larger, as seen in Fig. 9c, at approximately 8 h; this is while the moving average area values decrease over the seven-day propagation by approximately 1 m^2 (based on Fig. 8). These results confirm that the effect of time-varying area on the orbital decay of the debris accumulates over time. In Fig. 9c, the altitude vs. time plot of the long-term propagation is presented as a point of reference. The result for the 1* case included in Fig. 9a is significantly different from the other one-day simulations, and predicts a much earlier re-entry. This indicates the importance of the proper initialization of the spin axis, which must be in accordance with our understanding of its motion, as described in Section 3.2. These results quantify the effect of attitude motion on the re-entry predictions which becomes more significant as the spacecraft descends into altitudes where the atmospheric drag dominates its motion.

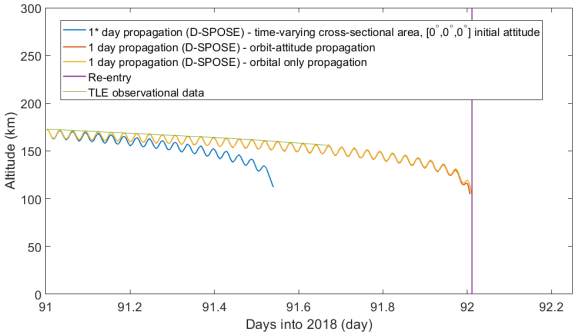

(a) Tiangong-1 position and attitude propagated from 1 day before re-entry

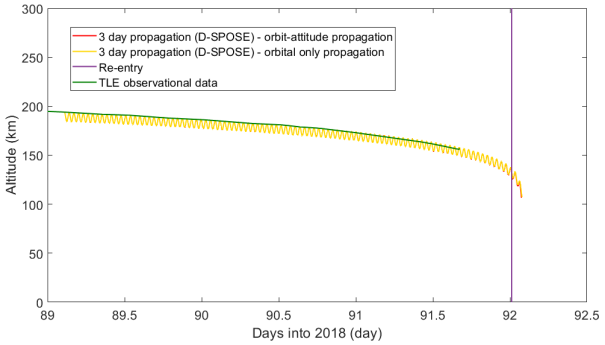

(b) Tiangong-1 position and attitude propagated from 3 days before re-entry

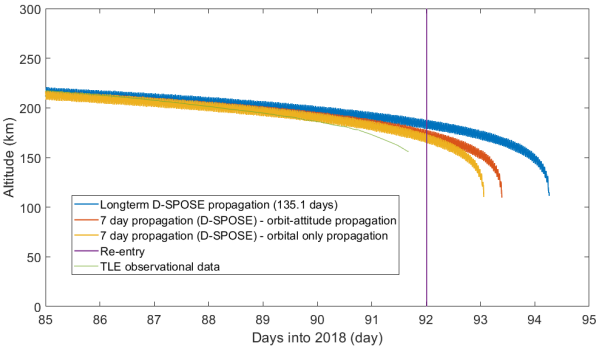

(c) Tiangong-1 position and attitude propagated from 7 days before re-entry

Figure 9: Tiangong-1 re-entry altitude vs. time

4.2. Effect of Average Cross-sectional Area on Impact Location

It is critical to note that the location of the debris at the point of re-entry varies due to the differences in descent time because of debris' rotational motion, as shown in

Table 1: Tiangong-1 initial conditions for short-term propagations with D-SPOSE

Length of Propagation (days)	Orbital Elements (from TLEs) [a,e,i,Ω,ω,θ]	Date and Time	Attitude (3-2-1 Euler angles) (deg)	Angular velocity (deg/s)
1	[6550.67,0.0019,42.76, 19.50,200.61,341.21]	01/04/2018 04:44:00	[-5.68,21.04,91.05]	[-0.09,-0.28,2.94]
1*	[6550.67,0.0019,42.76, 19.50,200.61,341.21]	01/04/2018 04:44:00	[0,0,0]	[-0.09,-0.28,2.94]
3	[[6571.73,0.0021,42.77, 15.58,213.20,344.43]	30/03/2018 02:38:00	[7.95,-26.38,78.34]	[0.07,-0.17,2.45]
7	[6595.73,0.0023,42.76, 358.12,241.04,1.90]	25/03/2018 21:00:00	[-176.80,24.33,-95.70]	[0.03,0.12,1.78]

Table 2: Tiangong-1 time of re-entry for short-term and long-term propagations predicted with attitude-orbital (time-varying area) and orbital only (fixed area) simulations using D-SPOSE

Length of Propagation (days)	Tiangong-1 Area (m^2)	Date and Time of Re-entry (d/m/y h:min)
135.1	Time-varying	04/04/2018 06:39
1	Time-varying	02/04/2018 00:19
1*	Time-varying	01/04/2018 12:39
1	28.36	02/04/2018 00:39
3	Time-varying	02/04/2018 02:08
3	28.33	02/04/2018 01:58
7	Time-varying	03/04/2018 10:10
7	28.58	03/04/2018 01:30

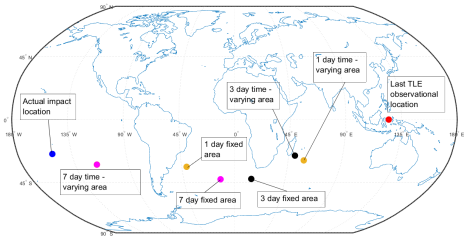

Figure 10: Tiangong-1 position after propagation using D-SPOSE (∼120 km altitude)

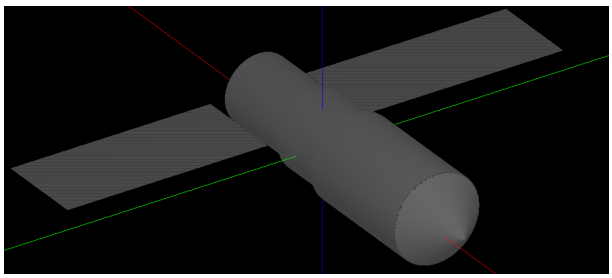

Figure 11: Debris geometry for simulation in DRAMA in body-fixed frame

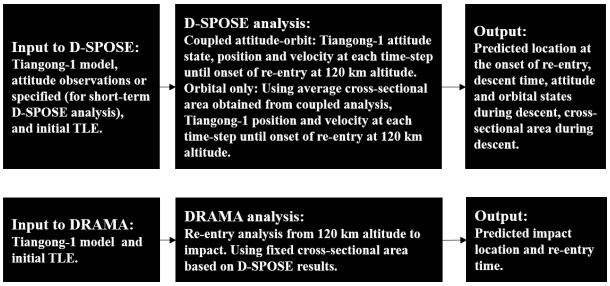

Figure 12: Schematics of D-SPOSE and DRAMA analyses

Fig. 10. To further analyse the effect this has on the impact location, the re-entry and risk analysis software DRAMA [4, 5] is employed in this section to predict the impact locations of Tiangong-1, based on the last published TLE of the station (observed on 01/04/2018 16:07:06). Presented in Fig. 11 is the Tiangong-1 geometry used for the DRAMA simulations. This model is generated for analysing the effect of the specified cross-sectional area on re-entry only. As such, the model is generated using the built-in function in DRAMA and therefore consists of basic shapes and is not tessellated nor tapered like the model employed in D-SPOSE simulations (Fig. 2). Similarly to the geometry presented in Section 2, the DRAMA geometry is generated based on dimensions provided in [6]. The solar panels are defined with the default "solar panel" material in DRAMA, and material for the rest of the model is defined as AA7075.

DRAMA3.0.3 [4] is employed to conduct the re-entry analysis from ∼120 km altitude (defined using the last recorded TLE on 01/04/2018 16:07:06) to impact, by using attitude-fixed, uncontrolled, and latitude band limited settings and with a value for the cross-sectional area of the station specified at input. In particular, five area val-

ues are considered in the range from 28 m^2 to 32 m^2, based on the moving average area values obtained from long-term propagation with D-SPOSE (as per Fig. 7, the last week of propagation). The drag coefficient used was the same as that for the D-SPOSE simulations ($C_D = 1.9$). The impact locations obtained using DRAMA are presented in Fig. 13. These results indicate that drastic variations in impact locations are predicted by specifying different values of the debris cross-sectional area, even varying them by only 10-15%, further supporting the importance of tracking and predicting debris attitude motion for re-entry analysis.

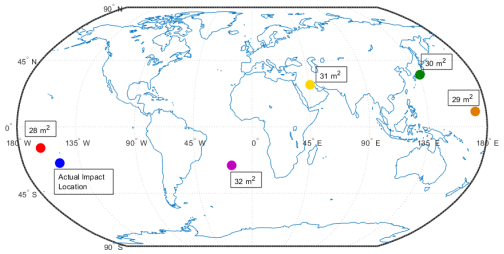

Figure 13: Tiangong-1 impact location predicted using DRAMA

4.3. Uncertainty in Solar Activity

As previously mentioned, it is suggested in [14] that a main source of uncertainty during a re-entry prediction campaign carried out three days prior to impact was the predicted solar activity. To study the effects of estimating solar activity during the final three days of descent, coupled orbit-attitude propagations are carried out using D-SPOSE with the actual solar indices measured during the last three days of Tiangong-1's re-entry compared to the same propagation, except with fixed solar indices. The values of the solar indices employed for both cases are presented in Table 3. The fixed values of the solar indices for the second propagation are taken as those measured three days before impact (on 30/03/18 in Table 3). Presented in Fig. 14 are the angular velocity and altitude responses during the last three days of descent of Tiangong-1, computed with fixed and actual solar indices. These results show only relatively minor differences, with the estimated time of impact varying by 1.4 hours between the two propagations. It is clear from these results that discrepancies in the predicted solar activity from actual solar activity over a three-day prediction time frame are not likely to be the cause of a 24-hour difference in the re-entry of the station, as was suggested in prior work [14]. It is important to note, however, that we are not able to make a direct comparison to the results in [14] because the solar index values used in that work were not reported.

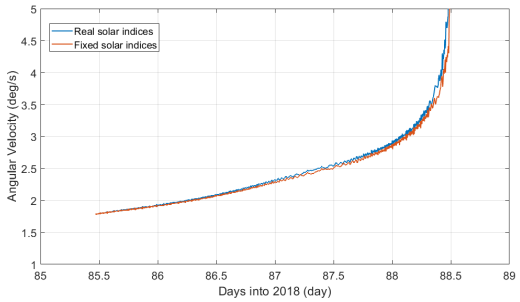

(a) Angular velocity

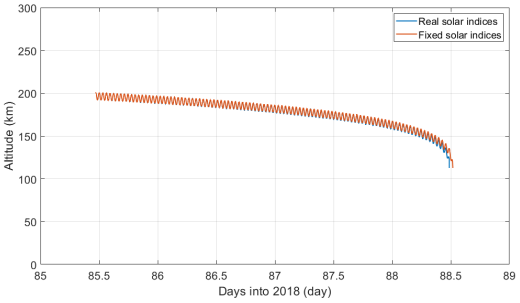

(b) Altitude

Figure 14: Effect of solar activity on altitude and angular velocity during the last three days of descent, obtained using orbit-attitude propagation with D-SPOSE

5. CONCLUSION

As Tiangong-1 descended towards re-entry at the beginning of 2018, observations from SLR and ISAR data showed an increase in its rotational velocity. As well, several observation and prediction campaigns to estimate the re-entry of the station were carried out through 2017 till the time Tiangong-1 impacted Earth in April 2018. In this paper, we employed the open-source coupled orbit-attitude propagation software D-SPOSE to analyze the attitude motion of the spacecraft during its final months of life in order to investigate its effect on the satellite's orbital motion and the consequent re-entry time and location predictions.

From the D-SPOSE simulation results, it was found that the software can accurately reproduce the evolution of the satellite's angular velocity, as seen by SLR and ISAR images, and that it is the complex interaction between the aerodynamic and gravity-gradient torques that produces the satellite's observed spin-up. Furthermore, the uncertainty and influence of the location of the center of mass and the satellite's major moment of inertia were assessed, thus allowing to suggest bounds on these values. With this information, the impact of the satellite's attitude dynamics on its orbital motion was put forward. Specifically, the satellite's mean cross-sectional area exposed to the incoming flow was found to decrease with time on the order of 20% over the last four months. This might explain discrepancies found in previous studies in long-term re-entry predictions of Tiangong-1 when a constant

Table 3: Fixed and actual solar index values for simulations of Tiangong-1 starting three days before re-entry

Propagation	Date (d/m/y)	$F_{10.7}$ (previous day)	$F_{10.7}$ (81-day average centred on current day)	Daily A_p Value
Fixed	30/03/18	69.0	69.04	4
Fixed	31/03/18	69.0	69.04	4
Fixed	01/04/18	69.0	69.04	4
Fixed	02/04/18	69.0	69.04	4
Actual	30/03/18	69.0	69.04	4
Actual	31/03/18	68.7	68.99	6
Actual	01/04/18	69.0	68.98	4
Actual	02/04/18	69.0	68.97	4

cross-sectional area was assumed and premature re-entry dates were obtained.

Using the likely parameter values identified from the focused investigation of the attitude dynamics of Tiangong-1, D-SPOSE software was then employed as a tool to investigate the effect of rotational motion on the orbital motion during the final days of descent. This was done with the view to understanding the implications of uncertainties in debris cross-sectional area on the accuracy of re-entry predictions. As such, simulations were carried out one-, three-, and seven-days before re-entry. On the very short-prediction time-scale (one to three days before re-entry), the results from coupled orbit-attitude propagation vs. orbit only propagation show similar re-entry times, where as the discrepancy in the seven-day predictions is much more significant. The effect on re-entry of small changes in cross-sectional area is further emphasised by the large differences in impact location found using DRAMA as a result of varying debris cross-sectional area by an amount corresponding to the variations revealed with the orbit-attitude propagation. Lastly, D-SPOSE results from varying solar indices between fixed and actual values, three days before re-entry, show a relatively small change in the re-entry time predictions. In light of these findings, we suggest that the debris rotational motion and the resulting changes in the debris' cross-sectional area over time are an important contributor to the accuracy of re-entry predictions and need consideration as much as other perturbations and uncertainties in orbit determination.

ACKNOWLEDGMENTS

The authors would like to thank Sommer et al. and the Fraunhofer Institute for High Frequency Physics and Radar Techniques for sharing their observational data and model of Tiangong-1, and Florent Deleflie for his insightful feedback and discussions. Furthermore, the authors are grateful to NSERC, Mitacs, FRQNT, Paris Observatory, IMCCE, and McGill University's Department of Mechanical Engineering for the funding and opportunities they provided.

REFERENCES

1. CHOI, E.-J., CHO, S., LEE, D.-J., KIM, S., AND JO, J. H. A study on re-entry predictions of uncontrolled space objects for space situational awareness. *Journal of Astronomy and Space Sciences 34*, 4 (2017), 289–302.
2. DELEFLIE, F., HAUTESSERRES, D., BERTHIER, J., CAPDEROU, M., AND PETIT, A. Atmospheric reentry predictions from tle long time series. application on the tiangong-1 reentry during spring 2018. *42nd COSPAR Scientific Assembly 42* (2018), PEDAS–1.
3. DROB, D. P., EMMERT, J. T., MERIWETHER, J. W., MAKELA, J. J., DOORNBOS, E., CONDE, M., HERNANDEZ, G., NOTO, J., ZAWDIE, K. A., MCDONALD, S. E., ET AL. An update to the horizontal wind model (hwm): The quiet time thermosphere. *Earth and Space Science 2*, 7 (2015), 301–319.
4. ESA. DRAMA software download. Website: `https://sdup.esoc.esa.int/drama/downloads`, 2020. Accessed: [April 21, 2020].
5. HTG. *DRAMA Final Report - Upgrade of DRAMA's Spacecraft Entry Survival Analysis Codes*, 1.0.2 ed. HTG,ESA, Am Handweisergraben 13, 37120 Bovenden, Germany, 2019.
6. LIN, H.-Y., ZHU, T.-L., LIANG, Z.-P., ZHAO, C.-Y., WEI, D., ZHANG, W., HAN, X.-W., ZHANG, H.-F., WEI, Z.-B., LI, Y.-Q., ET AL. Tiangong-1's accelerated self-spin before reentry. *Earth, Planets and Space 71*, 1 (2019), 1–9.
7. PARDINI, C., AND ANSELMO, L. Monitoring the orbital decay of the chinese space station tiangong-1 from the loss of control until the re-entry into the earth's atmosphere. *Journal of Space Safety Engineering 6*, 4 (2019), 265–275.
8. PAVLIS, N. K., HOLMES, S. A., KENYON, S. C., AND FACTOR, J. K. The development and evaluation of the earth gravitational model 2008 (egm2008). *Journal of geophysical research: solid earth 117*, B4 (2012).
9. PICONE, J., HEDIN, A., DROB, D. P., AND AIKIN, A. NRLMSISE-00 empirical model of the atmosphere: Statistical comparisons and scientific issues. *Journal of Geophysical Research: Space Physics 107*, A12 (2002), SIA–15.

10. SAGNIÈRES, L., AND SHARF, I. Long-term rotational motion analysis and comparison to observations of the inoperative envisat. *Journal of Guidance, Control, and Dynamics 42*, 2 (2019), 364–376.

11. SAGNIÈRES, L. *Modeling and Simulation of Long-term Rotational Dynamics of Large Space Debris*. PhD thesis, McGill University, 2018.

12. SOMMER, S., KARAMANAVIS, V., SCHLICHTHABER, F., PATZELT, T., ROSEBROCK, J., CERUTTI-MAORI, D., AND LEUSHACKE, L. Analysis of the attitude motion and cross-sectional area of Tiangong-1 during its uncontrolled re-entry. In *Proceedings of the 1st NEO and Debris Detection Conference* (2019), ESA Space Safety Programme Office Darmstadt, Germany.

13. VELLUTINI, E., BIANCHI, G., PARDINI, C., ANSELMO, L., PISANU, T., DI LIZIA, P., PIERGENTILI, F., MONACI, F., REALI, M., VILLADEI, W., ET AL. Monitoring the final orbital decay and the re-entry of tiangong-1 with the italian sst ground sensor network. *Journal of Space Safety Engineering 7*, 4 (2020), 487–501.

14. VIRGILI, B. B., LEMMENS, S., SIMINSKI, J., FUNKE, Q., AND FLOHRER, T. Combining observations for re-entry purposes. In *Advanced Maui Optical and Space Surveilance Technologies (AMOS) Conference* (2018).